Structural Dynamics of Cryogenic Target Assemblies

Introduction

The laser direct-drive approach to inertial confinement fusion (ICF) utilizes an array of high-power laser beams to uniformly compress a target capsule filled with hydrogen isotopes in a spherically symmetric implosion. Higher fuel densities, and therefore higher yields, may be achieved from targets that are filled with fuel under high pressure and cooled to form an ice layer on the inner surface of the capsule.[1] Cryogenic target assemblies for the OMEGA Laser System currently consist of a 900-μm-diam $\times$ 4- to 6-μm-wall glow discharge polymer (GDP) capsule[2] filled with a 100-μm layer of deuterium and tritium (DT) or deuterium (D_2) ice around a gaseous core. The capsule is suspended on four strands of spider silk from a beryllium frame[3] as shown in Fig. 108.15. During a typical implosion, laser illumination of the target rapidly heats and ablates the outer capsule material. Conservation of momentum drives the remaining capsule material and fuel toward the center of the target sphere where the initially gaseous fuel forms a "hot spot" that ignites fusion reactions, which propagate radially outward through the main fuel layer.[4]

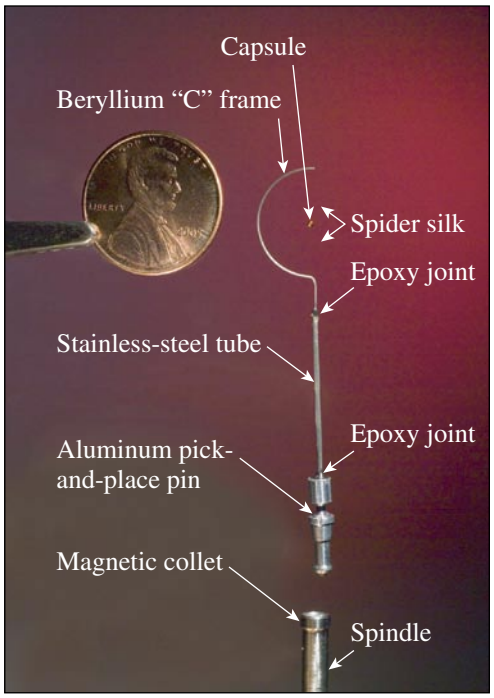

G7559JRC

Figure 108.15
OMEGA Cryogenic Target Assembly.

During an implosion, hydrodynamic instabilities in the ablation front can reduce the energy yield by distorting the hot spot or dispersing the main fuel layer. These instabilities, like Rayleigh–Taylor instability in classical fluids, initiate at small irregularities or perturbations in the ablation front. Asymmetries such as uneven laser illumination of the target or the presence of features on the outside surface of the capsule are potential triggers of instability during the acceleration phase of an implosion. While beam smoothing and power balancing can ensure highly uniform illumination at target chamber center (TCC),[5,6] target displacements of 5 μm or more[7] from TCC can unbalance the illumination enough to initiate hydrodynamic instability. Consequently, stringent requirements are imposed on the position of ICF targets at the time of implosion. Target-positioning systems must address both static and dynamic (oscillatory) displacements. While static displacements due to position control resolution, window offsets, and events such as removal of thermal shielding (shroud) immediately before firing the laser are a significant concern, they will be addressed in a future article.

In addition to meeting stringent position stability requirements, the mechanical supports for target capsules must also satisfy thermal and mass symmetry requirements. The mechanical supports must have a low thermal conductivity to minimize thermal gradients that perturb the ice layer within the capsule. Furthermore, the supports must not contribute a significant mass asymmetry to the capsule. Consequently, cryogenic target capsules for the OMEGA Laser System are suspended on four strands of spider silk that have a high modulus of elasticity (6.4 GPa), low density (1200 Kg/m^3), and is available in small diameters (0.9 μm), all of which minimize thermal and mass asymmetries. Furthermore, spider silk remains flexible at cryogenic temperatures.

The displacement amplitude of a capsule assembly is a function of the applied excitation force and the dynamic

response characteristics of the target assembly and surrounding structure. Numerous mechanical systems in and around the target chamber may generate periodic or transient forces that excite target vibration. Potential excitation sources include the cryogenic cooling system (helium compressor and cold head), vacuum pumps, solenoids, and forces applied by shroud retraction immediately before firing the laser. Continuously running systems such as induction motors typically excite vibration at discrete frequencies, whereas events that generate transient forces (impulses) such as opening and closing valves usually excite vibration over a broad frequency range. Either reducing excitation forces or isolating the target from the excitation is a very effective means for controlling target vibration, but doing so is not always practical. In such cases, the structural dynamics of the system become important.

The response of multidegree-of-freedom systems, such as the target assembly, to a given forcing function (F) is governed by a set of second-order differential equations so long as the stiffness remains constant; $M\ddot{X} + C\dot{X} + KX = F$. This set of equations relating the masses (M) of the degrees of freedom to the damping (C) and stiffness (K) linking the degrees of freedom constitutes an eigenvalue problem. Under the assumption of a harmonic response, the equations may be solved for eigenvalues that represent the natural frequencies of the system and associated eigenvectors that represent the relative displacement amplitudes of each degree of freedom or mode shape. To avoid high vibration amplitudes due to resonance, the natural frequencies must not coincide with those of forces that are strongly coupled with the associated mode shape. In situations where it is not possible to detune the natural frequencies from excitation sources, such as in the presence of broadband excitation, the vibration amplitude is then limited only by the system damping.

Finite element and experimental modal analyses are used to identify natural frequencies and characterize the associated mode shapes of cryogenic target assemblies for OMEGA. This information is used to interpret *in-situ* vibration data collected at TCC and to investigate the effect of proposed design changes on vibration.

Experimental Modal Analysis

Modal testing is a procedure for directly measuring the natural frequencies and mode shapes of a structure. For reasons of convenience, the target assembly was tested in air at room temperature and atmospheric pressure. A test article, identified as Cryo-ME-21, was constructed using a capsule with mass that is equivalent to a typical production capsule filled with hydrogen. It is important to note that the dynamic response characteristics under cryogenic conditions are likely to differ from those measured under the test conditions due to changes in the effective stiffness (strain) of the spider silk supporting the capsule and to the reduced damping under vacuum. Differential thermal expansion between the spider silk and beryllium frame and temperature dependence of the elastic moduli are expected to shift the natural frequencies of the target assembly. Material properties of the spider silk are not known at temperatures in the vicinity of the hydrogen's triple point.[8] The impact of cooling on a target's natural frequencies has not been studied in depth, but high-speed video of a few targets suggests that cooling the target increases the silk's natural frequencies by 0% to 7%.

A commercially available shaker system consisting of an electrodynamic actuator and a flexure table was used to excite vibration of the target assembly. The flexure table is intended to limit motion of the target base to translation in one direction. The target assembly was mounted on the shaker table with the beryllium C frame oriented at a 45° angle to the primary motion of the shaker so that both in-plane and out-of-plane modes of vibration could be excited simultaneously, as shown in Fig. 108.16. A random noise signal, capable of exciting vibration over the frequency range of interest up to 2 kHz, was used to drive the shaker at an amplitude of 25 μm, which is consistent with the excitation measured at TCC. Motion of the shaker (excitation) was measured using a piezoelectric accelerometer mounted at the base of the spindle, which connects the target assembly to the stalk (3 cm below the bottom of the pin shown in Fig. 108.15).

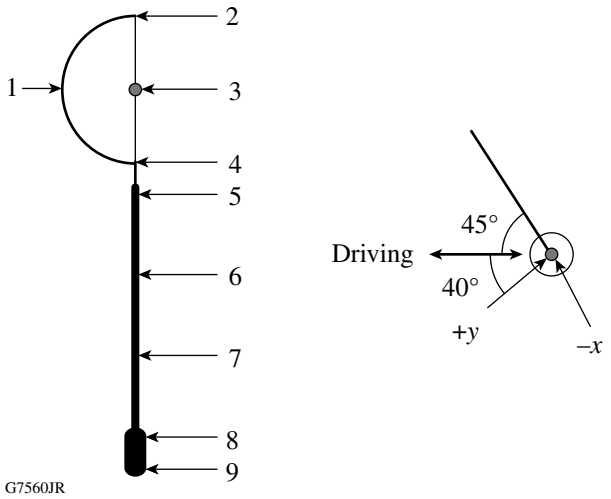

Figure 108.16
Measurement locations on target assembly.

The response of the target assembly to the applied base excitation was measured at the nine points shown in Fig. 108.16. A laser vibrometer was used to measure velocity of each point in two orthogonal directions corresponding approximately to in-plane (x) and out-of-plane (y) of the beryllium C frame. Use of an optical measurement method, as opposed to mounting accelerometers on the target assembly, is necessary to avoid adding mass that would change the natural frequencies of the target assembly.

Data from the test were processed using a multichannel dynamic signal analyzer to compute H1 frequency response function (FRF) estimates[9] that represent the amplitude and phase of the response as functions of frequency. In the FRF calculation, the amplitude at a given frequency is normalized by dividing the response (velocity) of each point on the structure by the excitation (acceleration) at a common reference location on the shaker table. To prevent errors in the fast Fourier transformation (FFT), which forms the basis for this calculation, a weighting window was applied. Discontinuities between the beginning and end values of nonperiodic signals were suppressed by a Hanning window, which reduces the signal amplitude at the beginning and end of the sampling interval. The FRF amplitudes were scaled to resolve the excitation force into the target x and y directions, which were oriented at approximately 45° angles to the excitation. Transmissibility functions were calculated for each measurement point by differentiating the FRF's to produce nondimensional amplitude ratios. Figure 108.17 shows composite transmissibility functions that were created by averaging the transmissibility amplitudes in each direction.

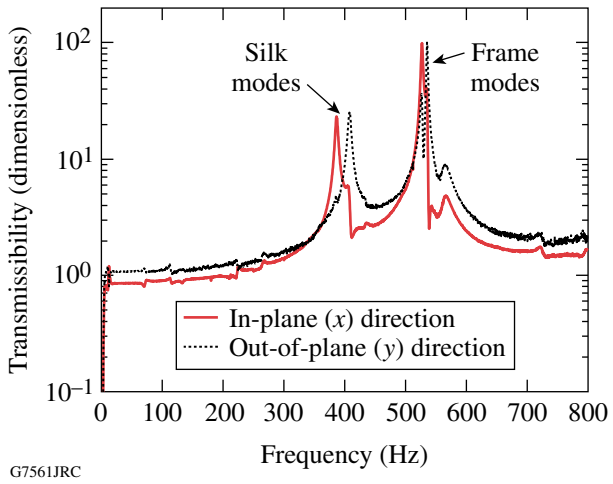

Figure 108.17
Target assembly transmissibility.

The transmissibility functions from the target assembly were analyzed using Polymax[10] curve-fitting functions to extract natural frequencies, modal damping values, and associated mode shapes. Graphically, the peaks in the transmissibility function indicate natural frequencies, and the relative amplitudes correspond to the mode shapes. Highly damped modes have lower and broader peaks in the transmissibility function. Curve fitting the transmissibility data identified the four stable modes listed in Table 108.I, where damping is expressed both as a percentage of critical and as an exponential decay time constant. At these natural frequencies, the coherence of all the measurements is greater than or equal to 95%. The other peaks in the spectrum (most notable at 570 Hz) are artifacts of secondary axis motion by the shaker.

Table 108.I: Experimental modal analysis results.

Mode	Frequency (Hz)	Damping	Description
1	386	0.6% (0.07 s)	In-plane silk translation
2	408	0.6% (0.07 s)	Out-of-plane silk translation
3	526	0.5% (0.06 s)	In-plane frame bending
4	535	0.1% (0.30 s)	Out-of-plane frame bending

Figure 108.18 shows the mode shapes associated with the four natural frequencies. The relative amplitude and direction of vibration at each measurement location are indicated by arrows. Mode 1 (386 Hz) and mode 2 (408 Hz) are dominated by translation of the capsule in and out of the plane of the C frame under silk tension. In tests on 16 mass-equivalent targets, the natural frequency of the silk mode in the y direction is consistently greater than in the x direction (with an average separation of 24 Hz). In mode 3 (526 Hz) and mode 4 (535 Hz) the mode shapes are dominated by bending of the C frame in plane (x) and out of plane (y) with the capsule moving out of phase with the frame.

Analytical Modal Analysis

A finite-element model of the target assembly was created to predict its dynamic response characteristics. To validate the model, boundary conditions, damping, and room-temperature material properties were used to predict the natural frequencies and mode shapes measured experimentally. Once validated, uses for the model include studies of the sensitivity to variation in uncertain parameters (such as spider silk properties), evaluation of proposed design changes, and prediction of the response

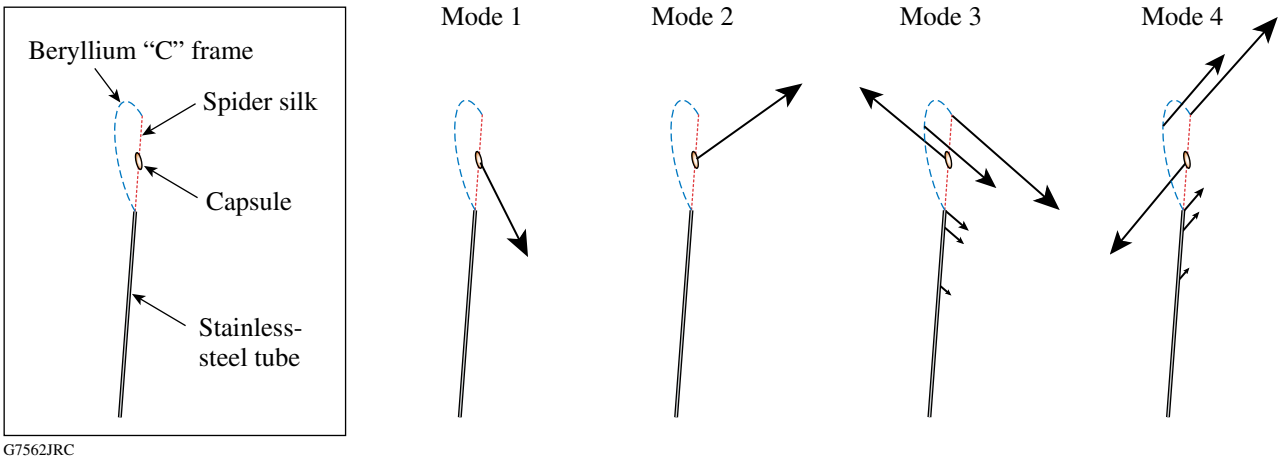

Figure 108.18
Experimental mode shapes.

characteristics under cryogenic conditions (if material properties such as Young's modulus, density, and coefficient of thermal expansion are determined or adequately approximated).

Construction of a Finite-Element Model

The target assembly consists of six relatively simple components (capsule, spider silk, beryllium C frame, stainless-steel tubing, the pin, and adhesives). Material properties for the components are listed in Table 108.II. Damping ratios from the experimental modal analysis results were applied to the model. In general, the system is assumed to respond in a linear manner or approximate a linear response for limited displacements. Specific modeling assumptions and methods for the components are described in the following sections.

Table 108.II: Material properties.

Material	Young's modulus (GPa)	Poisson's ratio	Density (kg/m^3)
Spider silk[6]	6.4	0.24	1200
Stainless steel[11]	193	0.29	7800
Aluminum[11]	70	0.33	2700
Beryllium[11]	300	0.10	1850
Epoxy[11]	5.0	0.35	1550

1. Target Capsule

The target capsule was modeled as a rigid body using a point mass element. Before assembling the target used for the experimental modal analysis (Cryo-ME-21), the capsule mass, outside diameter, and wall thickness were measured to be 56 μg, 878 μm, and 25 μm, respectively. It should be noted that the test article has the same outside diameter and a greater wall thickness than production targets to make its mass equivalent to a DT-filled production capsule. The capsule geometry and mass were used to calculate the rotational moment of inertia about an axis through its center of mass. The rotational inertia of the adhesive attaching the capsule to the four strands of spider silk was assumed to be negligible. While the mass of the test article is the same as that of a filled production target, the rotational inertia will differ because the density of GDP is over 3.5 times that of DT ice. While the rotational inertia of the mass-equivalent capsule is 14% greater than a typical production capsule filled with DT ice, the modes of interest, which consist primarily of translation, are not significantly affected.

The capsule was connected to four spider silks via a series of eight stiff, zero-mass beam elements. Each beam ran from the point mass to contact points on the outer surface of the capsule as measured under a microscope. The separation between the silk contact points in the horizontal (xy) plane may vary by up to 10 μm due to ambiguity in the assembly process. Figure 108.19 shows a magnified view of the target-point mass and how it is assembled to the spider silk in the finite-element model.

2. Spider Silk Modeling

The spider silk strands were modeled using link elements that act in tension only. During the assembly process, tension is applied to each strand of silk by stretching to a nominal strain of 5.6%. With the strain below the yield point, the modulus of elasticity was assumed to be constant. The four silk strands supporting the capsule were collected from a single "drop line," which has been shown to have consistent properties over its entire length.[8] Specimens from the same drop line were

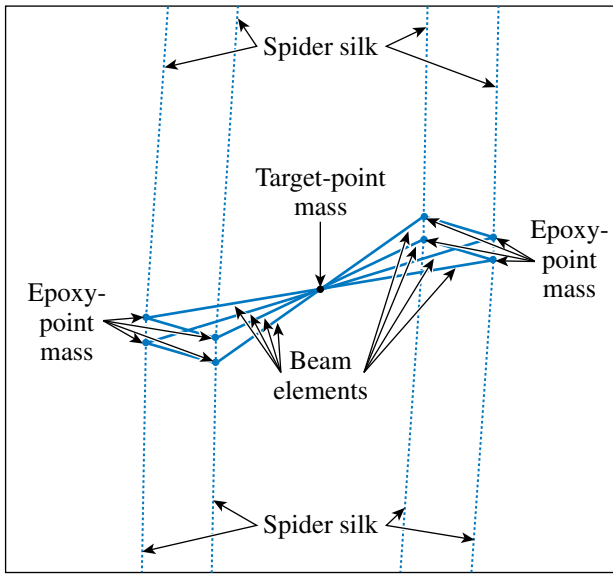

Figure 108.19
The target-point-mass assembly in the finite-element model.

analyzed under a scanning electron microscope to determine the number of fibers and their cross-sectional area. Another specimen from the same drop line was tested to determine its modulus of elasticity.

The silk was attached to the target, as shown in Fig. 108.19. Small, stiff, zero-mass beams were used to create the attachment point between the silk and the beryllium C frame. The beams ran from the center of the beryllium wire to the theoretical tangential contact points between the outside diameter of the wire and the silk. Figure 108.20 shows how the model was created. Figure 108.21 is a geometric representation of element size and configuration.

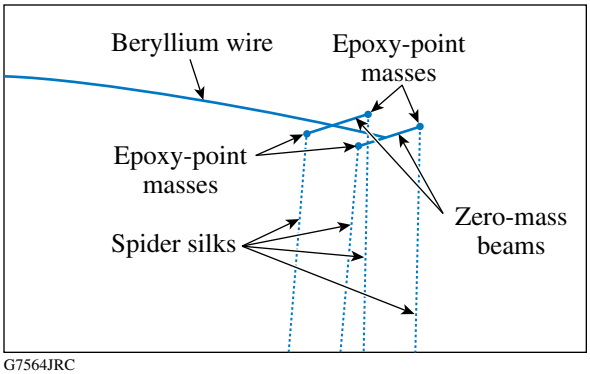

Figure 108.20
Silk beryllium connection mass.

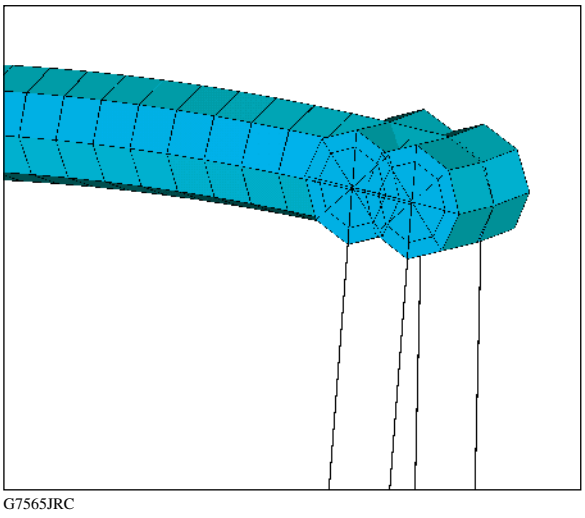

Figure 108.21
Silk beryllium connection elements.

3. C Frame and Support Tube

Beam elements were used to model the wire frame that supports the spider silk and the tube that connects the frame to the pin. The beryllium-wire C frame was assumed to have a round cross section with a constant diameter determined by measuring the test article. The stainless-steel support tube was assumed to have a circular cross section with constant diameter and wall thickness based on nominal values from the manufacturer.

4. Support Pin and Collet

The support pin at the bottom of the target assembly was modeled using a six-degrees-of-freedom beam element. The magnetic collet joint that attaches the target assembly to the spindle was assumed to be very stiff and was modeled by constraining the pin to the spindle (excitation source) in all six degrees of freedom. If the assumption of an ideal collet joint is not valid, the predicted natural frequencies of the first bending mode will be higher than the measured values. Excitation from the shaker was simulated by applying a harmonic acceleration to the collet in the x and y directions.

5. Epoxy Joints

Epoxy joints connecting the beryllium C frame to the stainless-steel tube and the stainless-steel tube to the pick-and-place pin were modeled using six single-degree-of-freedom spring elements. The springs were created between two coincident nodes. Half of the mass of the epoxy joint was applied to each of the coincident nodes. Figure 108.22 shows a cross section of a representative pin joint. The C-frame joint was not analyzed due to hazards associated with machining beryllium. During assembly, the tube is pushed against one side of the hole in the pin as shown in Fig. 108.22.

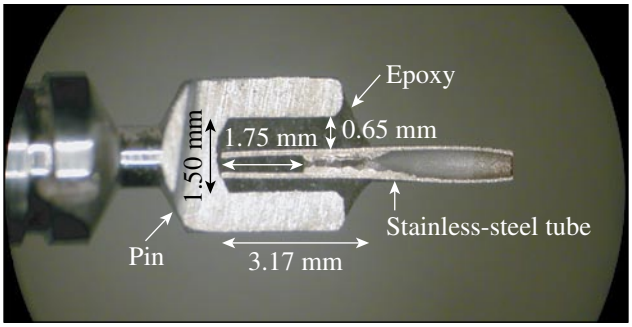

Figure 108.22
Cross section of pin and stainless steel tube.

Likewise, the beryllium wire is pushed against the side of the tube in the positive x direction as shown in Fig. 108.23. Detailed finite-element models of the epoxy joints were used to assess their stiffness in each direction. Forces and bending moments were applied individually in each direction, and solutions were obtained for the resulting displacements. The effective stiffness of the joint was calculated and applied to the corresponding spring elements in the target model; however, the mass and stiffness of epoxy in the joints may vary from target to target.

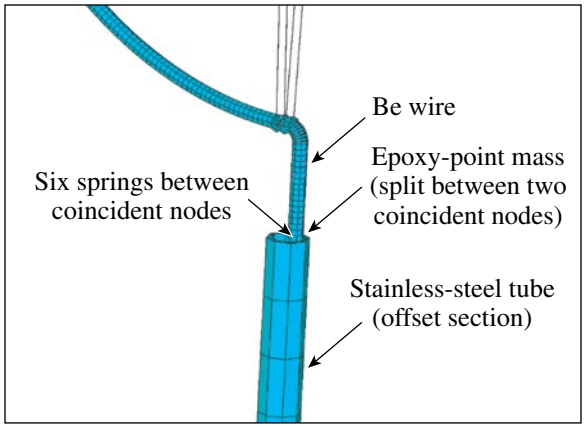

Figure 108.23
Beryllium wire connection to stainless-steel tube.

Analysis Results

The model was used to calculate the dynamic response characteristics of the target assembly at room temperature. Natural frequencies and associated mode shapes of the target assembly were calculated through modal analysis of the model. Damping values from the experimental modal analysis results, which represent both structural and aerodynamic affects, were applied to the model. A harmonic analysis based on superposition of the response to a sine sweep was used to calculate the frequency response function shown in Fig. 108.24.

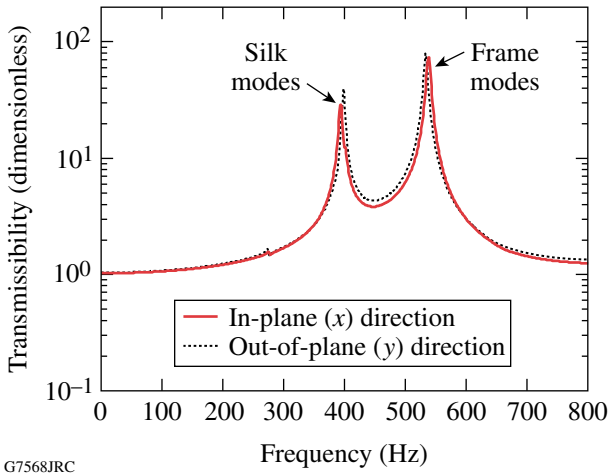

Figure 108.24
Transmissibility functions.

Correlation of Analytical and Experimental Results

The model was validated by comparing the predicted frequencies and mode shapes with the experimental values. Table 108.III shows the correlation between the measured natural frequencies and the corresponding predicted values. Prediction of frequencies within 3% of the experimental values suggests that the model is valid for assessments of potential design changes and sensitivity studies.

Table 108.III: Natural frequency correlation.

Mode description	Experimental frequency (Hz)	Analytical frequency (Hz)	Difference
In-plane (x) silk translation	386	393	1.9%
Out-of-plane (y) silk translation	408	400	–1.9%
In-plane (x) frame bending	526	538	2.3%
Out-of-plane (y) frame bending	535	535	0.0%

The mode shapes associated with the largest peaks in the FRF's are similar to the experimental results presented in Fig. 108.18. At 278 Hz, the model predicts a mode dominated by the capsule spinning about the z axis with an orbital component that produces translation when the geometric center of the silk/capsule contact points is offset from the capsule's center of mass. The laser vibrometer used in the experiment measures only translation and is therefore not well suited to detect the first mode. While a small peak in the experimental FRF (268 Hz) corresponds closely with the predicted frequency of the first rotational mode, the peak

is attributed to a mode of the shaker. Modal assurance criteria (MAC)[12] are used to compare the predicted and experimental mode shapes dominated by translation of the measurement points. A scalar MAC value is calculated for each pair of analytical and experimental mode shapes to determine their consistency. Fundamentally, the MAC values are based on "R^2" correlation coefficients used in linear regression. A MAC value close to 100% indicates a high degree of correlation, and a value close to zero indicates uncorrelated modes. The MAC matrix shown in Table 108.IV indicates that the predicted mode shapes correlate closely with the experimental modes shapes at corresponding frequencies (diagonal terms in the matrix).

Table 108.IV: Modal assurance criteria.

		Experimental			
Frequency (Hz)		386	408	526	535
Analytical	393	93	16	16	12
	400	6	84	11	18
	538	26	0	84	17
	535	0	26	16	82

The separation between the *x*- and *y*-direction silk modes near 400 Hz is affected by a variety of parameters including the silk attachment offset from the capsule center of mass, the distance between adjacent points, and uneven silk tension. However, the cumulative effect of improved model fidelity in these areas separates the silk modes by only 7 Hz and does not explain the measured 22-Hz separation. Furthermore, the fact that the out-of-plane silk mode consistently has a higher natural frequency (24±6 Hz on average for mass-equivalent targets) suggests that a systematic source of asymmetry remains unmodeled. However, none of the experimental data collected to date suggests a correlation between the gain (amplitude) and frequency separation of the silk modes.

The model predicts a natural frequency of the in-plane, frame-bending mode, which is higher than the out-of-plane mode. While the experimental results presented here contradict the model's prediction, data from eight similar mass-equivalent targets support the prediction. On average the in-plane mode has a natural frequency that is higher by 0.6±5.9 Hz. This variability is consistent with sensitivity studies performed on the quantity and distribution of adhesive and assembly tolerances in the epoxy joints.

Applications

Information gained from the study of target dynamics is being used to understand and reduce capsule vibration at TCC. During simulated shots (without firing the laser), the vibration of mass-equivalent target capsules has been measured with high-speed video (HSV) cameras. Analysis of the data from two cameras with roughly orthogonal views yields three-dimensional capsule displacements at frequencies up to 1 kHz. The broadband vibration amplitude varies from 5 to 100 μm at the time when the laser would fire (less than 100 ms after retraction of a thermal shroud that maintains the capsule at 20 K). Auto-power spectra functions calculated from the HSV data indicate that capsule displacement is typically dominated by vibration at a few discrete frequencies, as shown in the spectrum from a representative target in Fig. 108.25. The HSV measurements and modal test were performed on different targets. The *x*- and *y*-direction, silk-mode natural frequencies of the target from which the HSV data were collected were 254 and 275 Hz, respectively, and the frame-mode natural frequencies were 592 and 589 Hz, respectively. Two peaks in the HSV auto-power spectrum (270 and 291 Hz) correspond very closely with the silk-mode natural frequencies. A 10-Hz decrease in the frequencies of these two peaks during the first few seconds after shroud removal suggests that the governing stiffness decreases quickly (probably due to warming of the spider silk). Based on observation of similar sets of corresponding peaks from other targets (at different frequencies), these peaks in the HSV auto-power spectra are attributed to the silk modes. However, the frame modes, which do not typically appear in the HSV data, are either not excited or are more heavily damped. Consequently, efforts to control target vibration at TCC need to focus on the silk modes and the peaks around 50 Hz, which are not attributable to the target assembly. The modes around 50 Hz are not discussed in this work.

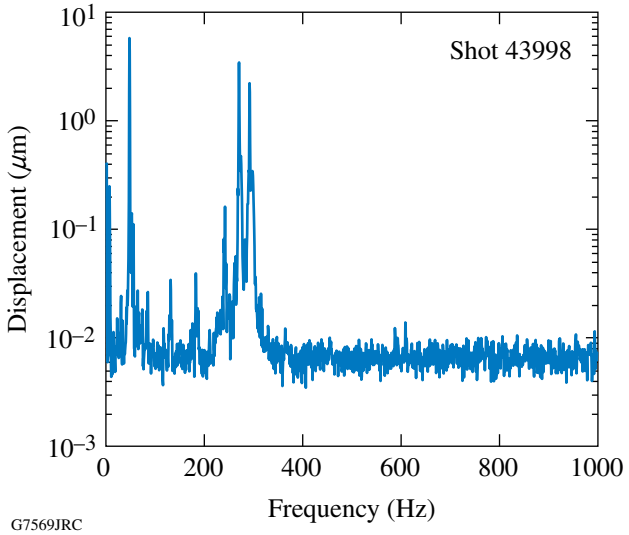

Figure 108.25
High-speed video spectrum.

Frequency response functions of production targets are measured at one location (the capsule) for quality-assurance purposes before filling the capsule with fuel. The silk-translation natural frequencies of the 66 targets produced from May through September 2006 ranged from 650 Hz to over 1200 Hz. Note that the empty capsule has considerably less mass and therefore higher silk-translation natural frequencies than the mass-equivalent target. The silk-translation modes of empty production targets are also more heavily damped when tested on the shaker due to the reduced mass and increased velocity. The frame-mode natural frequencies of production targets are typically very close to those of mass-equivalent targets. Figure 108.26 shows an FRF from a representative production (target ID Cryo-2062-669) target with an empty capsule.

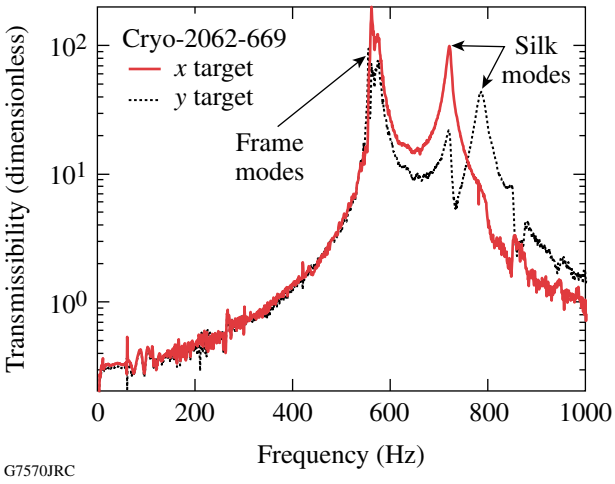

Figure 108.26
Experimental FRF of an empty production target capsule.

The finite-element model was used to predict the dynamic response characteristics of the production target (Cryo-2062-669) once the empty capsule was filled with either 33 μg of D_2 or 42 μg of DT fuel. The model, which does not account for thermal effects, predicts silk natural frequencies of 410 and 450 Hz when filled with D_2 and 380 and 415 Hz when filled with DT. The impact of cooling on target natural frequencies has not been studied in depth, but high-speed video of a few targets suggests that cooling the target increases the silk natural frequencies by 0% to 7%. Once cooled, the target is expected to have natural frequencies of 455 and 495 Hz if filled with D_2 and frequencies of 420 and 455 Hz if filled with DT.

Variability in the spider silk dimensions and material properties is an unfortunate consequence of working with a naturally occurring material. Sensitivity of the target assembly dynamics to variations in the spider silk properties was investigated with the finite-element model. For an unfilled target, Fig. 108.27 shows the predicted variation in natural frequency of the first translational silk mode as a function of strain, silk modulus, silk diameter, and capsule mass. For an initial strain of 5.6% (the nominal value in the current production process),

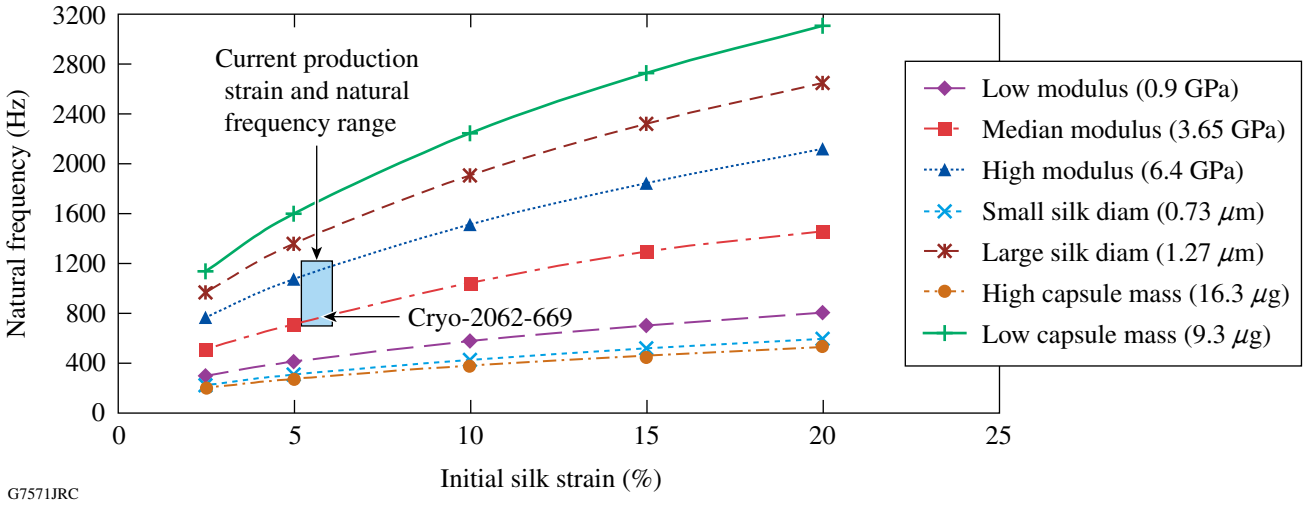

Figure 108.27
Silk mode sensitivity to strain, modulus, diameter, and capsule mass.

the natural frequency of the first silk translation mode can vary by approximately 670 Hz due to a three-standard-deviation variation in the elastic modulus.[8] Variation in the diameter of the silk (three standard deviations) increases the range to 1050 Hz. Variations in capsule wall thickness from 3.6 μm to 6.3 μm affect the silk translation natural frequencies by changing the mass (9.5 to 16.5 μg) and increasing the range of natural frequencies to 1330 Hz.

The predicted mean and standard deviations of silk-mode natural frequency based on the sensitivity analysis (920±220 Hz) are greater than the values (865±160 Hz) obtained from measuring the natural frequencies of the 66 targets produced from May through September. However, the experimental bandwidth of the shaker was limited to 1200 Hz, and applying this constraint to the FEA data (under the assumption of a Gaussian distribution) reduces the range to 910±201 Hz. Future target-frequency-response tests will have a 2-kHz bandwidth that encompasses the three-standard-deviation range of silk-mode frequencies. The discrepancy between the predicted and measured frequency ranges indicates that the effective modulus of the tested targets is lower and more consistent than published values. Seasonal effects on silk properties may broaden the experimental uncertainty bounds; these will be studied in the future.

Filling the targets with D_2 or DT fuel changes the predicted (three-standard-deviation) range of silk-mode natural frequencies (assuming 5.6% initial strain) to 150 to 750 Hz, and 130 to 670 Hz, respectively. The variation in silk-mode natural frequencies could be reduced by adjusting the silk strain during target fabrication to compensate for variations in silk properties. However, the elastic modulus measurement process employed in this study would not be practical for routine use in target fabrication. For the purpose of tuning the silk-mode natural frequencies, a more expedient and less accurate measurement would suffice.

Overlap between the frequency ranges for the frame and silk translation modes presents the possibility of coupling between the modes. As a silk mode and a frame mode approach the same frequency, the associated mode shapes shown in Fig. 108.18 become increasingly similar. The effect of coupling was investigated as a potential cause for high vibration of some production targets. Interaction between the modes is measured in terms of the target capsule's transmissibility value (gain) at the natural frequencies. The FRF's in Fig. 108.28 illustrate the effect of increasing the silk-mode natural frequency. In addition to increasing the gain of both silk and frame modes, coupling also shifts the frame-mode frequencies higher by roughly 75 Hz. Figure 108.29 shows the gain of the frame and silk modes plotted as functions of the silk-mode natural frequency. When the silk-mode natural frequency coincides with that of the frame modes (526 Hz and 538 Hz), coupling increases the frame-mode gain by a factor of 4 and the silk-mode gain by a factor of 2 with respect to the measured silk-mode natural frequency (400 Hz).

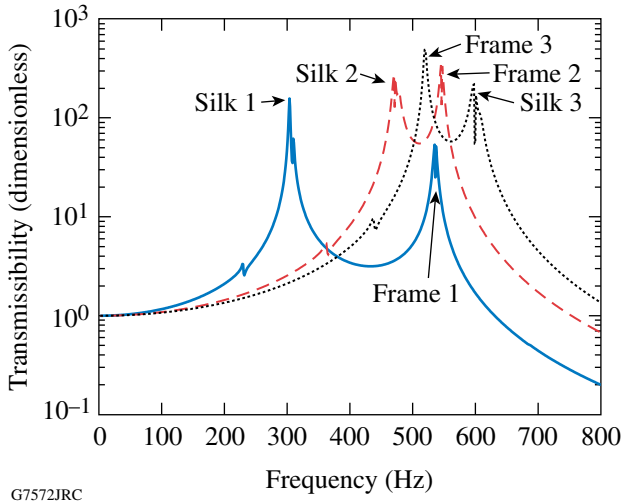

Figure 108.28
FRF's showing coupling effect.

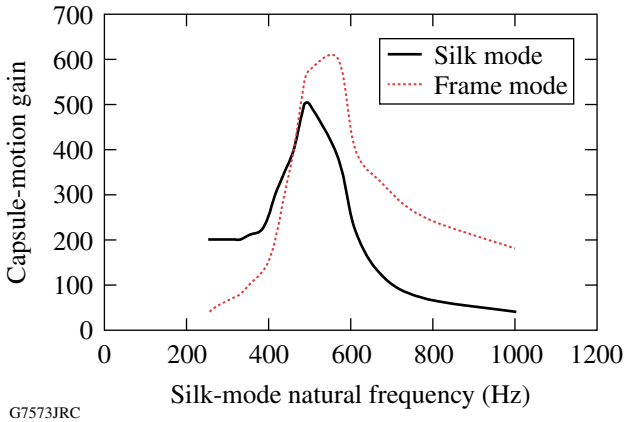

Figure 108.29
Silk- and frame-mode coupling.

To prevent coupling, acceptance criteria will be established for an empty target's natural frequencies. The single-degree-of-freedom model shown on p. 180 provides simple and accurate (based on correlation with the finite-element model) predictions of the silk-mode natural frequencies of a fully fueled target (f_{full}) based on the measured natural frequency when

empty (f_{empty}). Targets with fully fueled silk natural frequencies between 85% and 125% of the frame natural frequencies will be rejected.

$$f_{\text{full}} = f_{\text{empty}} \times \sqrt{\frac{\text{capsule mass}}{\text{capsule mass + fuel mass}}}. \quad (1)$$

Analysis of the HSV data reveals several clues regarding the excitation. First, excitation of silk translation modes in targets with silk natural frequencies ranging from 270 to 570 Hz indicates the presence of a broadband excitation source such as an impulse or random noise. Second, the absence of vibration at the frame-mode natural frequencies implies weak coupling between the excitation source and frame modes or high damping of the frame modes. Potential excitation sources including shroud separation forces and target clearance to the thermal shroud during retraction are currently being investigated.

Conclusion

The analytical model predicts natural frequencies of translation modes within 3% of those obtained experimentally. Correlation of target capsule vibration at TCC with the target dynamic response characteristics obtained from this study indicates that the silk modes are a primary cause of capsule displacement during shots. While increasing the silk-mode natural frequencies would typically reduce the displacement amplitude, coupling between the silk and frame modes is believed to counteract the benefits until the silk-mode frequencies are significantly greater than those of the frame modes. Increasing the silk natural frequencies would probably introduce significant mass asymmetry. Therefore, the authors are designing a new cryostat that will not excite the silk modes and are exploring stiffer capsule-support concepts.

ACKNOWLEDGMENT

This work was supported by the U.S. Department of Energy Office of Inertial Confinement Fusion under Cooperative Agreement No. DE-FC52-92SF19460, the University of Rochester, and the New York State Energy Research and Development Authority. The support of DOE does not constitute an endorsement by DOE of the views expressed in this article.

REFERENCES

1. T. C. Sangster, J. A. Delettrez, R. Epstein, V. Yu. Glebov, V. N. Goncharov, D. R. Harding, J. P. Knauer, R. L. Keck, J. D. Kilkenny, S. J. Loucks, L. D. Lund, R. L. McCrory, P. W. McKenty, F. J. Marshall, D. D. Meyerhofer, S. F. B. Morse, S. P. Regan, P. B. Radha, S. Roberts, W. Seka, S. Skupsky, V. A. Smalyuk, C. Sorce, J. M. Soures, C. Stoeckl, K. Thorp, J. A. Frenje, C. K. Li, R. D. Petrasso, F. H. Séguin, K. A. Fletcher, S. Padalino, C. Freeman, N. Izumi, J. A. Koch, R. A. Lerche, M. J. Moran, T. W. Phillips, and G. J. Schmid, Phys. Plasmas **10**, 1937 (2003).

2. A. Nikroo *et al*., General Atomics, San Diego, CA, GA–A23881 (2002).

3. D. T. Goodin *et al*., in *Proceedings of the 17th IEEE/NPSS Symposium on Fusion Engineering* (IEEE, New York, 1997), Vol. 1, pp. 309–312.

4. J. D. Lindl, Phys. Plasmas **2**, 3933 (1995).

5. P. W. McKenty, V. N. Goncharov, R. P. J. Town, S. Skupsky, R. Betti, and R. L. McCrory, Phys. Plasmas **8**, 2315 (2001).

6. D. D. Meyerhofer, J. A. Delettrez, R. Epstein, V. Yu. Glebov, V. N. Goncharov, R. L. Keck, R. L. McCrory, P. W. McKenty, F. J. Marshall, P. B. Radha, S. P. Regan, S. Roberts, W. Seka, S. Skupsky, V. A. Smalyuk, C. Sorce, C. Stoeckl, J. M. Soures, R. P. J. Town, B. Yaakobi, J. D. Zuegel, J. Frenje, C. K. Li, R. D. Petrasso, D. G. Hicks, F. H. Séguin, K. Fletcher, S. Padalino, C. Freeman, N. Izumi, R. Lerche, T. W. Phillips, and T. C. Sangster, Phys. Plasmas **8**, 2251 (2001).

7. R. S. Craxton, ed. *OMEGA Upgrade Preliminary Design*, Laboratory for Laser Energetics, University of Rochester, Rochester, NY, LLE Document No. DOE/DP 40200-101 (1989).

8. M. J. Bonino, "Material Properties of Spider Silk," M.S. Thesis, University of Rochester, 2003.

9. J. S. Bendat and A. G. Piersol, *Engineering Applications of Correlation and Spectral Analysis* (Wiley, New York, 1980).

10. LMS International, Leuven, Belgium.

11. A material properties database, MatWeb is a division of Automation Creations, Inc., Blacksburg, VA 24060, December 2006, http://www.matweb.com (11 December 2006).

12. R. J. Allemang and D. L. Brown, in *Proceedings of the International Modal Analysis Conference & Exhibit* (Society for Experimental Mechanics, Schenectady, NY, 1982), pp. 110–116.